

Using periodic line fires to gain a new perspective on multi-dimensional aspects of forward fire spread

R.R. Linn^a, J.M. Canfield^{a,*}, P. Cunningham^a, C. Edminster^b, J.-L. Dupuy^c, F. Pimont^c

^a Earth and Environmental Sciences Division, Los Alamos National Laboratory, Los Alamos, NM 87545, USA

^b United States Forest Service, Rocky Mountain Research Station, Flagstaff, AZ 86001, USA

^c Institut National pour la Recherche Agronomique, Unité de Recherches Forestières Méditerranéennes, Equipe de Prévention des Incendies de Forêt, UR 629, F-84914 Avignon, France

ARTICLE INFO

Article history:

Received 2 September 2011

Received in revised form 13 January 2012

Accepted 14 January 2012

Keywords:

Coupled atmosphere–fire modeling

Three-dimensional dynamics

Fire spread

ABSTRACT

This study was conducted to increase understanding of possible roles and importance of local three-dimensionality in the forward spread of wildfire models. A suite of simulations was performed using a coupled atmosphere–fire model, HIGRAD/FIRETEC, consisting of different scenarios that varied in domain width and boundary condition implementation. A subset of the simulations was strictly two-dimensional in the streamwise and vertical directions, while another subset of simulations involved igniting a finite-length fireline. The remaining simulations were all three-dimensional and employed periodic boundary conditions in the cross-stream direction and a fireline spanning the entire cross-stream extent of the domain.

The three-dimensional periodic simulations were compared with the two-dimensional simulations, and then briefly with the finite-length fireline simulations. The two-dimensional scenarios were constrained in their ability to represent inherently three-dimensional physical phenomena such as horizontal flow penetrating through the fireline between plumes of rising hot gas, and cross-stream heterogeneity in the windfield. Elimination of these three-dimensional flow patterns in two-dimensional simulations resulted in over prediction of spread rates in low velocity situations and under predicted spread rates in high wind speed scenarios. In the three-dimensional simulations, local cross-stream heterogeneities in temperature and velocities lead to penetration of hot gases through the fireline and onto unburned fuel. Three-dimensional fires presented a positive correlation between increasing ambient wind speed and rate of spread. Further investigation of finite length fires is required in order to understand the ramifications of fireline curvature.

Published by Elsevier B.V.

1. Introduction

Frequent low-intensity fires have historically been beneficial phenomena in wildland environments, clearing away excessive growth and regulating the competition for finite resources. However, a century of fire suppression has left our forests choked with fuel that has been dried to tinder by years of drought, and now when natural fires occur they are often catastrophic (Brown and Arno, 1991). It is widely appreciated that the more we understand about wildfire behavior, the more we can anticipate dangerous situations or environmental impacts, and the more we enable intelligent decisions regarding fuels and fire management as well as risk

mitigation. For this reason there is an increasing need to understand wildfire behavior and its response to environmental conditions.

1.1. Objective

The objective of this paper is to use a three-dimensional coupled atmosphere–fire model to examine the ramifications of ignoring the influence of the local cross-stream heterogeneities when modeling fire behavior. Idealized scenarios are combined with a creative use of boundary condition techniques to isolate the local impacts of the three-dimensional physics present in and around the fireline. Three-dimensional fires are simulated with fuel, ignition, and incoming winds that are completely homogeneous in the cross-stream direction. Cyclic boundaries are used to remove any effects of fireline curvature or end effects. This boundary condition treatment has been shown to be useful to simplify the study of fuel treatment effects by removing influences of end effects (Pimont et al., in press; Cassagne et al., 2011). One of the most important realizations about the differences between the simulations with

* Corresponding author.

E-mail addresses: rrl@lanl.gov (R.R. Linn), jessec@lanl.gov (J.M. Canfield), pcunning@lanl.gov (P. Cunningham), cedminster@fs.fed.us (C. Edminster), dupuy@avignon.inra.fr (J.-L. Dupuy), pimont@avignon.inra.fr (F. Pimont).

cyclic boundary conditions and those with finite-length or broken firelines is that in the former the wind is unable to move around the fireline, and there are no flanking portions of the fire. The results of these simulations are compared to two-dimensional fires (vertical plane) under the same environmental conditions, in order to suggest the significance of this effect on spread rate.

The plan of the present paper is as follows. Section 1 summarizes some of the approaches that have been used by the wildfire community to study fires. In Section 2, we provide a brief summary of the coupled atmosphere–fire model, along with a description of the suite of numerical simulations that will be used to explore the impacts of three-dimensionality of atmosphere–fire coupling. In Section 3, the results of these simulations and their interpretations are described. In Section 4, the implications of the results are presented along with an outline of more in-depth studies arising from the present paper.

1.2. Wildfire research tools

The wildfire research community uses wildfire behavior models to augment expert opinions, experiments, and field observations in the hope of identifying some of the relationships between various environmental conditions, such as winds or local vegetation structure, wildfire processes and fire behavior. Modeling wildfires is difficult because wildfire behavior is determined by an extremely complex set of coupled processes that occur over a very wide range of length and time scales. There are a variety of types of models that are being developed within the community, along with an equally wide variety of assumptions, simplifications, and approximations, that are used in order to close these models and to achieve the various levels of desired detail and speed in calculations. Amongst the models that are currently being advanced for wildfire research, there are several, including WFDS (Mell et al., 2007), FIRESTAR (Larini et al., 1998; Morvan and Dupuy, 2001), FIRETEC (Linn, 1997; Linn and Cunningham, 2005), and the models proposed by Zhou et al. (2005) and Grishin (1997), that attempt to represent important physical processes including fluid flow and heat transfer, with the goal of capturing the essence of the driving forces and simulating the resulting wildfire behavior.

One of the most prominent features of wildfire behavior is the speed at which it moves in various directions. The speed of advancement of a fire in the direction of the wind, referred to as the heading-fire spread rate and in this text as simply spread rate, is a result of the interaction between a variety of processes including heat transfer, moisture evaporation, and combustion rates. In this regard, arguably the best known dependence of fire on its environment is the relationship between the heading-fire spread rate and the wind speed in that direction, which has been demonstrated both by laboratory experiments (e.g., Carrier et al., 1991; Wolff et al., 1991; Weise, 1993; Catchpole et al., 1998) and by field experiments (e.g., Cheney et al., 1993, 1998; Cheney and Gould, 1995). The basic concept that the wind in the direction of the fire spread controls the spread in that direction has led many modelers to attempt to model fire spread in terms of the wind speed in the direction of spread. In some cases, one-dimensional theoretical models have been developed based on perceived governing physical relationships (Koo et al., 1997). In other cases, researchers have combined empiricism and physical relationships to model fire behavior in this one-dimensional context connecting wind and topographic slope to spread in the same direction (Cheney et al., 1998; Dupuy and Larini, 1999; Rothermel, 1972). Indeed, wind speed has a leading-order impact on wildfire behavior. Nevertheless, the dynamics associated with the dependence of wildfires on the ambient wind speed, the influence of fire-induced flow patterns, and the complex balances between physical processes in the fire that change with the local wind, are still not well understood

(e.g., Baines, 1990; Beer, 1991, 1993; Linn and Cunningham, 2005; Cunningham and Linn, 2007).

It is impossible to model all of the physical processes in the context of just one dimension; however, these simplified models have provided impressive results in some wildfire contexts (e.g., Rothermel, 1972). Some of these models were later extended to two-dimensional horizontal planar models such as FARSITE (Finney, 1998). Others were explored by Margerit and Séro-Guillaume (2002). These horizontal plane models provided estimates of fire front movement in all horizontal directions across a landscape, but the spread vectors are still local functions of mean wind speed and topographic slope in the direction of spread.

Researchers have tried to use computational fluid dynamics techniques to explore the relationship between forward wildfire spread and ambient winds. Early investigations in this regard were constrained by computational costs, leading scientists to attempt to simulate atmosphere–fire interactions using a two-dimensional x – z plane, where x is the direction of the wind and spread and z is the vertical direction, based on an assumption that the fire is very long and straight (homogeneous) in the third dimension (Linn, 1997; Morvan and Dupuy, 2001). In these models, the dependence of spread rate on wind speed is not predetermined, but is instead a self-determining result of the interaction between the modeled physical processes. The results of these models indicate spread rates that increase with wind speed for moderate winds; however, the spread rate is not steady, even in constant winds, and seems to behave counter-intuitively for high wind speeds, even decreasing with wind speeds at high winds (Morvan and Dupuy, 1997). For interpretation of the results provided by these models, it is important to consider the two rather different contexts under which a fire can be represented in a two-dimensional framework. The first context is a scenario where the fireline is very long (assumed to be infinitely long, or that any end effects can be ignored) and nominally straight. In this context, much like two-dimensional turbulence approximations, the general assumption is that the impact of mean cross-stream components of wind velocities and heat fluxes for any (x, z) location can be represented in terms of quantities that are averaged over the length of the fireline. This assumption does not preclude local fluctuations from these mean values, including local gusts in the cross-stream direction, vorticity in the x - or z -directions, or hot and cool spots along the fireline with associated local variations in cross-stream heat fluxes, as long as the mean values are zero and the local details of such cross-stream details may be ignored. This assumption in the two-dimensional model configuration does prevent the explicit representation of such details. The challenge of describing the fire behavior in this context is to account for unresolved impacts of local variability on the overall fire behavior without resolving them. This situation is directly analogous to the impact of turbulence over a very long obstacle in a cross flow: the mean flow parallel to the length of the obstacle might be zero, but this does not mean that at sufficiently high Reynolds numbers the flow does not exhibit fully three-dimensional turbulent structures or flow fields that affect the development and sustainability of the wake behind the obstacle. The mean flow will have only two-dimensional aspects, but the turbulent statistics would show the presence of significant energy being redirected into local fluctuations and heterogeneities in the third dimension. These localized fluxes in the cross-stream direction have an impact on the recovery of the velocities in the wake region, and it is important to account for their impact on the overall flow even though the mean value of the local fluctuations is zero when averaged over the length of the obstacle. The second context that can be considered two-dimensional is one in which the fireline is infinitely short and there is no cross-stream distance for variations or fluxes in the third direction. The thought model for this scenario might be a fire that is pinched between two pieces of frictionless glass with just enough

room for air to pass between them in the streamwise and vertical directions. In this case, not only is the average velocity in the cross-stream direction zero, but there are no fluctuations in this direction either. This notion of fire would result in a flat, unbroken sheet of flame spanning the length of the fireline (conceptually, the distance between the plates). Unfortunately, by default fire models that are implemented in just two dimensions, such as that described in Linn (1997), are more representative of this second scenario than of the infinitely long case, since they did not account for the kinetic energy or net impacts of the local cross-stream fluxes and heterogeneities (although Linn (1997) did account for some of the unresolved fine scale hydrodynamic fluctuations through the turbulence closure scheme). Simple observations of wildland fires demonstrate that, regardless of the nature of the winds or the straightness of the fireline, there are always variations in the instantaneous flame shape along the length of the fireline (Beer, 1991). In other words, the fire does not look like a perfect sheet of flame standing up from the burning fuel, but instead looks like a multitude of intermittent jets that are out of phase with each other. Computational fluid dynamics techniques have also been used to explore the interaction between buoyancy sources and ambient winds. In these numerical experiments, the interaction between buoyant heat sources and ambient winds is inherently three dimensional, even in cases where attempts are made to create situations that are idealized and unrealistically two-dimensional in terms of upwind velocities, surface roughness, and heat sources (e.g., Cunningham et al., 2005). In light of the fact that there are computational advantages to simulating fires using one-dimensional or two-dimensional (vertical plane) models, it is important to understand the significance of the additional degrees of freedom obtained from the third dimension (cross-stream direction). Similarly, it is equally important to understand the constraints imposed by omitting the third dimension.

Recent papers (i.e., Linn and Cunningham, 2005; Mell et al., 2007; Cunningham and Linn, 2007) have simulated grass fires using three-dimensional coupled atmosphere–fire models. In most of these studies, the grass fuel beds were at least locally homogeneous (although Mell et al. (2007) included fuel breaks on the edge of simulated experimental plots) on scales many times the thickness of the simulated firelines. Given the homogeneity of the fuels, the perpendicular nature of the wind to the ignited fireline, and the uniformity of winds in these simulations, there might be an expectation that fires would propagate nearly uniformly, or at least in a nominally one-dimensional mode (at least in the middle of the firelines); however, a variety of three-dimensional features were observed in the simulated firelines and winds. These features included local variations in fireline geometry and intensity as well as fire-scale curvature of the fireline. In this regard, it is important to note that the fire-scale curvatures in Mell et al. (2007) were in some cases influenced by the fact that the authors had paid special attention to igniting the simulated fires as they had been ignited in the Australian grass fire experiments they were attempting to reproduce, and in doing so had given the center of the fire a head start on the outside edges of the fire.

In Linn and Cunningham (2005) and Cunningham and Linn (2007), a coupled atmosphere–fire model, referred to as HIGRAD/FIRETEC or more briefly FIRETEC (Linn, 1997; Linn and Harlow, 1998; Reisner et al., 2000), was used to investigate basic fire behavior in homogeneous grasslands. Some of the simulated fires were ignited from 16 m long firelines, and others from 100 m long firelines, using an idealized ignition technique that started fire along the entire length of the line simultaneously. These simulated fires also showed local heterogeneity and overall fire-scale curvature even though the ignition had been performed in a more idealized and less-realistic manner (compared to Mell et al. (2007)). The simulations described by Linn and Cunningham (2005) illustrated how a set of physical processes might collectively result

in the dependence of forward spread rate on wind speed, as did Mell et al. (2007). The spread rates of the simulated fires in these papers corresponded closely to those found in the field experiments described by Cheney et al. (1993) and Cheney and Gould (1995). These simulations also suggested that the overall size and shape of simulated fires in weak wind conditions were significantly different from those seen in simulations with stronger winds.

These differences in fire behavior between weak wind and strong wind conditions were attributed by Linn and Cunningham (2005) to differences in the nature of the coupled atmosphere–fire interactions occurring at different wind speeds, and specifically to the interplay between radiative and convective heat transfer at different wind speeds. Cunningham and Linn (2007) described the simulated evolution of the heat transfer mechanisms and the turbulent coupled atmosphere–fire interactions in detail, along with the impacts of local fireline orientation with respect to the wind (i.e., forward and lateral spreading portions of the fire).

Previous research has demonstrated the computational advantages of using one-dimensional or two-dimensional (vertical plane) approaches to modeling fire behavior. Nevertheless, both experiments (Alexander et al., 2004) and results from recent physics-based three-dimensional modeling efforts (Mell et al., 2007; Linn and Cunningham, 2005; Linn et al., 2005a; Pimont et al., in press; Dupuy et al., in press) suggest that the inherent three-dimensionality of the coupled atmosphere–fire interaction might make it difficult to predict fire behavior – or even head fire spread rates – without accounting for at least the presence of local cross-stream heterogeneity in physical processes. In this paper we are specifically interested in the local fire-line scale heterogeneities and three-dimensionality.

2. Methods and strategy

The strategy behind this investigation is to use FIRETEC to simulate: (1) fires in two-dimensional configurations where there are no local fluxes or heterogeneities in the cross-wind direction (resembling the infinitely short fireline described above); and (2) fires in three-dimensional configurations where the local cross-stream fluxes and heterogeneities are not held to zero, but the integrated fluxes in the cross-stream direction are zero and the fireline can be thought of as infinitely long with no end effects. These simulations will be compared for reference purposes with a set of simulations of fires ignited from finite-length firelines, where winds are allowed to move around the lateral extent of the fires.

2.1. Model description

HIGRAD is an atmospheric computational fluid dynamics (CFD) model that was specifically designed to represent coupled atmospheric processes that frequently involve sharp gradients in velocities, concentrations, or temperatures. HIGRAD uses a fully compressible finite-volume formulation and its development has been driven by application to a wide variety atmospheric phenomena including hurricanes, urban and explosive dispersion, and coupled turbine/atmosphere processes for wind energy harvesting.

The ability to model wildfires is created by coupling a wildfire behavior model, FIRETEC, to HIGRAD in such a way as to have two-way exchange between FIRETEC and HIGRAD in terms of: mass (fire emissions); energy (combustion energy release, convective and radiative heat transfer, and heat of evaporation of moisture); and momentum (vegetation drag). FIRETEC includes representation of three-dimensional heterogeneous fuel beds, multiscale turbulence, net combustion processes and energy release. The FIRETEC model is a multi-phase transport model, based on the ensemble-averaged conservation equations for mass, momentum, energy,

and chemical species. FIRETEC incorporates treatments of the macroscale effects of processes such as combustion, radiation, convective heat exchange, and aerodynamic drag in order to achieve a self-determining coupled atmosphere–fire model. The physical and chemical formulations of the model have been described in detail in several previous publications (Linn, 1997; Linn and Harlow, 1998; Linn et al., 2002; Linn and Cunningham, 2005; Colman and Linn, 2007; Pimont et al., 2009), and the details are not repeated here. This combined HIGRAD/FIRETEC simulation tool, hereafter referred to as simply FIRETEC, provides a vehicle to study the exchange of forcing that the atmosphere puts on the fire and that the fire puts on the atmosphere as well as the implications for fire behavior.

FIRETEC was developed with the intension of modeling many of the critical physical phenomena that control the behavior of a wildfire and their interactions through a set of coupled partial differential equations. FIRETEC simulates the interaction between the physical processes by explicitly resolving many of them through a finite volume numerical solution algorithm and stochastically representing others through subgrid models for those fine-scale processes and heterogeneities that cannot be resolved. FIRETEC has been used to simulate historical fires (Bossert et al., 2000; Bradley, 2002) and field experiments (Linn et al., 2005b; Linn and Cunningham, 2005; Pimont et al., 2009) and continued efforts to further validate if for broader sets of scenarios are underway. FIRETEC has been applied as a tool to study basic fire behavior phenomena (Linn et al., 2005a, 2007, 2010; Pimont et al., 2006, in press; Cunningham and Linn, 2007; Parsons, 2007; Cassagne et al., 2011; Dupuy et al., in press). The applications of FIRETEC span ecosystems from sparse grass to heavily forested woodlands on both flat terrain and rugged topography and include the interaction between fire and canopy structure and the interaction between multiple firelines.

It should be noted that FIRETEC is quite computationally expensive to and is not faster than real time. In addition this sort of detailed CFD-based fire behavior model requires much more explicit details concerning the three-dimensional structure of the heterogeneous vegetation and wind fields surrounding the fire. The speed of calculations and data requirements dictate that even though such models have the potential to provide insight into the coupled processes in wildfire behavior, they are not appropriate for real time use or by those that are not familiar with this sort of modeling. For this reason FIRETEC is considered a research tool and is not widely used by fire managers.

2.2. Set up of simulations

In Table 1, cases that end in '2D' are two-dimensional vertical x – z plane simulations with no thickness in the y -direction and with ambient winds of 1, 3, 6, 9, 12, and 15 m s^{-1} , respectively. In these simulations, there are not multiple grid cells in the y -direction, therefore there can be no variability in this direction. These are the simulations that can be imagined as fire burning between two frictionless reflective planes that are very close together.

Cases that end in '10m', '20m', '40m', '80m', and '160m' are three-dimensional simulations with periodic boundary conditions in the cross-stream or y -direction. Periodic boundary conditions, which are also referred to as cyclic boundary conditions, create a situation where fluxes passing out through the right boundary pass in through the left boundary and vice versa. The result of this type of boundary is a domain in which the cross-stream computational boundary location is completely arbitrary because the simulated domain becomes just one segment of an infinite number of identical segments, and each segment links up to adjacent segments as consistent as if the seam were in the interior of a computational domain. This approach allows heterogeneities of local flux structures up to the size of the domain width. When

Table 1
Simulation parameters.

Simulation	Ambient speed, U_{10m} (m s^{-1})	Domain size (x, y) (m)	Ignition length (m)
U01FINITE	1.0	960 × 320	100.0
U01y2D	1.0	1280 × –	–
U01y10	1.0	1280 × 10	10.0
U01y20	1.0	1280 × 20	20.0
U01y40	1.0	1280 × 40	40.0
U01y80	1.0	1280 × 80	80.0
U01y160m	1.0	1280 × 160	160.0
U03FINITE	3.0	960 × 320	100.0
U03y2D	3.0	1280 × –	–
U03y10	3.0	1280 × 10	10.0
U03y20	3.0	1280 × 20	20.0
U03y40	3.0	1280 × 40	40.0
U03y80	3.0	1280 × 80	80.0
U03y160m	3.0	1280 × 160	160.0
U06FINITE	6.0	960 × 320	100.0
U06y2D	6.0	1280 × –	–
U06y10	6.0	1280 × 10	10.0
U06y20	6.0	1280 × 20	20.0
U06y40	6.0	1280 × 40	40.0
U06y80	6.0	1280 × 80	80.0
U06y160m	6.0	1280 × 160	160.0
U09FINITE	9.0	960 × 320	100.0
U09y2D	9.0	1280 × –	–
U09y10	9.0	1280 × 10	10.0
U09y20	9.0	1280 × 20	20.0
U09y40	9.0	1280 × 40	40.0
U09y80	9.0	1280 × 80	80.0
U09y160m	9.0	1280 × 160	160.0
U12FINITE	12.0	960 × 320	100.0
U12y2D	12.0	1280 × –	–
U12y10	12.0	1280 × 10	10.0
U12y20	12.0	1280 × 20	20.0
U12y40	12.0	1280 × 40	40.0
U12y80	12.0	1280 × 80	80.0
U12y160m	12.0	1280 × 160	160.0
U15FINITE	15.0	960 × 320	100.0
U15y2D	15.0	1280 × –	–
U15y10	15.0	1280 × 10	10.0
U15y20	15.0	1280 × 20	20.0
U15y40	15.0	1280 × 40	40.0
U15y80	15.0	1280 × 80	80.0
U15y160m	15.0	1280 × 160	160.0

studying the influence of allowing or disallowing local variability in the y -direction, and local fluxes of momentum and heat in this direction, it is important to consider the fact that the size scales of the local fluctuations could have an impact on the larger-scale fire behavior. In order to assess the potential for this impact, a variety of domain widths were used to allow heterogeneities to develop at a variety of scales. Domains of 10, 20, 40, 80, and 160 m wide, with periodic boundaries in the cross-stream direction, were employed for each of the six different ambient wind speeds. This series of simulations also allows for the size of important three-dimensional atmospheric structures to change with wind speed. It should be mentioned that the three-dimensional structures in the periodic simulations result from nonlinear processes, such as the hydrodynamics that are described by the Navier–Stokes equations, interacting with any small perturbations in the cross-stream (y) direction. If these simulations were run with no perturbations in the y -direction (i.e., initial and boundary conditions perfectly homogeneous in the y -direction) the simulations would remain completely homogeneous in the y -direction, producing a computationally expensive two-dimensional simulation (unless computational round-off errors perturb the symmetry). Since nature always exhibits perturbations in winds, fuels, and any kind of fire ignition, a weak, $O(10^{-3} \text{ m s}^{-1})$, 4 m wide pin-wheel like vortex perturbation was placed in the initial conditions within the interior of the domain. This perturbation dissipates quickly

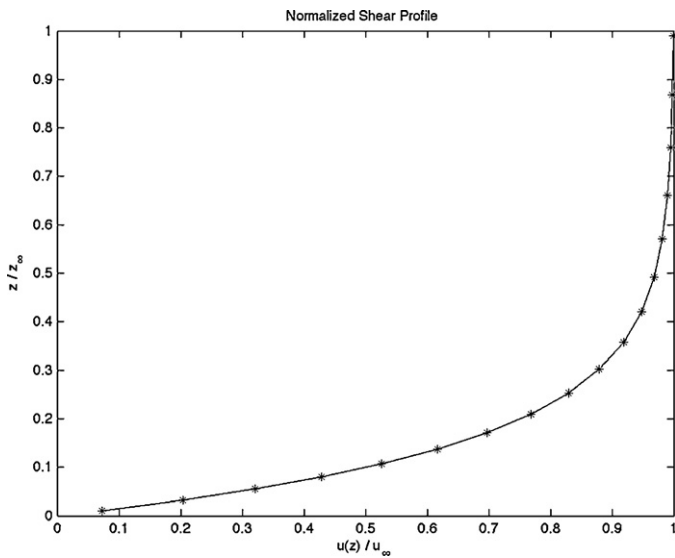


Fig. 1. Here is an example of the shear profile in the first 70 m above the ground for $U(z)$ normalized by U_∞ .

once the simulation begins, but the small disturbance is enough to engage the nonlinear flow dynamics and generate the fully three-dimensional nature of the fire and flow fields that are depicted in Fig. 2.

In all of the simulations described in this paper, the grid spacing in both of the horizontal directions is uniform and equal to 2 m, and in the vertical direction is nonuniform, with a grid spacing near the ground of approximately 1.5 m increasing to about 30 m at the top of the domain at $z=615$ m. The height of the domain was chosen to achieve an optimal balance between minimizing the interaction between the strong buoyancy flows and the top of the domain and minimizing the computational cost. The horizontal domain sizes for the various simulations are shown in Table 1. In all simulations, the fuel bed load is specified to be similar to tall grass of height 0.7 m, with a load of 0.7 kg m^{-2} , contained within the first grid cell above the ground. Within the fuel bed, the surface area per unit volume is specified as 4000 m^{-1} , which is typical for tall grass (e.g., Rothermel, 1972; Burgan, 1988), and has been used by others (Cheney et al., 1993; Linn and Cunningham, 2005), and the initial fuel moisture fraction (i.e., the mass of water divided by the mass of fuel) is 0.05. The ambient atmospheric stability is taken to be neutral in all cases, and the Coriolis parameter is neglected. Environmental wind profiles were specified using an exponential expression, defined by $U(z) = U_\infty(1 - e^{-z/z_0})$, where U_∞ is the ambient upstream velocity above the ground and z_0 is a reference height of 10 m. This velocity profile monotonically increases from zero at the ground and asymptotes to U_∞ above the ground. At the reference height, z_0 , the velocity is approximately 65% of U_∞ . Fig. 1 depicts an example of this profile for $U(z)$ normalized by U_∞ . For the purpose of clarity, it should be emphasized that this profile is different from the less realistic uniform inlet wind profile used by Linn and Cunningham (2005), and so comparison of spread rates with these previous FIRETEC simulations must be performed with care.

3. Results and discussion

There are many ways to characterize fire behavior and numerous quantities that can be examined from the output of a coupled atmosphere–fire model such as FIRETEC. It is possible, as in Linn and Cunningham (2005), to describe the nature of the overall trends including rate of spread and fire shape. It is also possible to

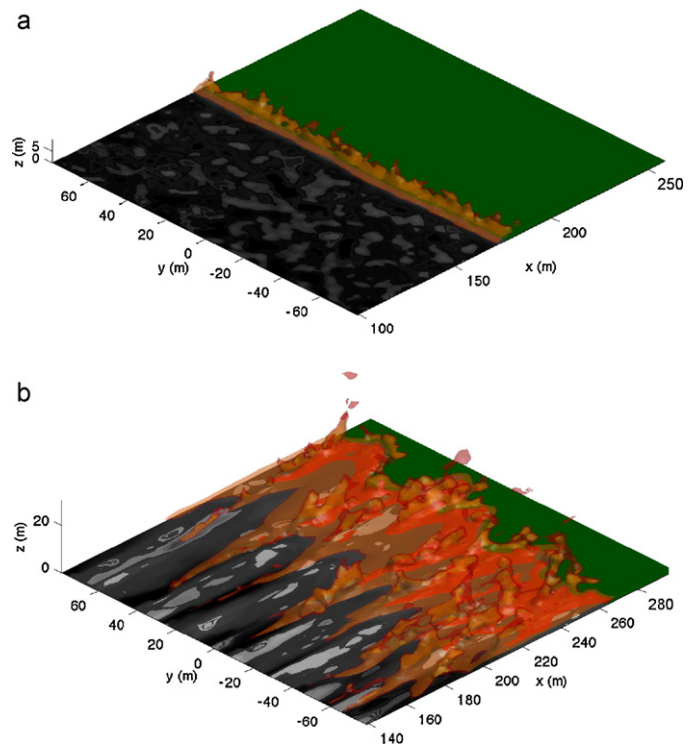


Fig. 2. These images show isosurfaces of potential temperature (500 K – pale orange, 600 K – red) and oxygen concentration (0.05 – bright orange) for: (a) U01y160m at $t=800$ s, and (b) U06y160m at $t=200$ s. The horizontal surface depicts solid fuel depletion (green indicates zero depletion, black indicates near full depletion).

delve quite deeply into the correlations between various physical properties, and to dissect the details that combine to produce the larger-scale physical processes. Within this paper, the description of the results is limited to local three-dimensionality and its effect on fireline propagation with a specific focus on rate of spread. The details of the coupled fire/atmosphere interactions will be presented in subsequent publications because of the extensive discussion required to explain those aspects of the results.

3.1. Global ambient wind effects

Fig. 2 illustrates the three-dimensional periodic firelines from simulations U01y160m and U06y160m using potential temperature isosurfaces at 500 K (pale orange), 600 K (red), and oxygen concentration isosurfaces at 0.05 (bright orange). The complicated shape of these surfaces, and the presence of variation in the y -direction is typical for all of the periodic simulations that were performed, although the details and amplitudes of the structures are specific to each wind speed and to a lesser extent the width of the domain. Each x – z slice within the domain is different from the others as a result of local non-zero fluxes in the y -direction. There are significant differences in the structure of the fires for the 160 m wide simulations between the case with ambient winds of 1 m s^{-1} (Fig. 2a) and those with ambient winds of 6 m s^{-1} (Fig. 2b). In Fig. 2a, the U01y160m fire can be seen to have a relatively narrow streamwise cross-section in comparison to the U06y160m fire. This trend is consistent with the results described in Table 2. Another significant difference between these images is the fact that the isosurfaces in Fig. 2a are much more vertical in nature than those seen in Fig. 2b. This is an expected effect of the higher wind speeds in the latter case; however, it should be noted that the degree to which the flame is tilted by the wind is also variable in the y -direction.

Table 2

Spread rates for each scenario. The first column represents the ambient wind speed at a height of 10 m above the ground. The second column has the spread rates for a finite length fire line. The third through eighth columns contain spread rates for the two-dimensional and periodic fire lines.

Wind speed U_{10m} ($m s^{-1}$)	100 m finite	2D	10 m	20 m	40 m	80 m	160 m
1.00	0.13	0.57	0.25	0.23	0.22	0.22	0.22
3.00	0.67	1.10	1.33	1.35	1.25	1.18	1.14
6.00	1.13	1.24	2.15	2.27	2.14	1.91	1.92
9.00	1.64	0.77	2.23	2.81	2.41	2.49	2.28
12.0	2.36	0.76	2.67	3.14	2.96	2.94	3.01
15.0	2.74	1.63	3.17	3.31	3.56	3.47	3.44

3.2. Local wind effects and horizontal fireline geometry

Fig. 3a–c shows plan views from the U01y160m, U06y160m and U12y160m simulations, respectively, where vectors have been used to illustrate flow fields at a height of 0.75 m above the ground, and solid and dashed contour lines depict the positions of gas hotter than 350 K and 400 K. In addition, these images include straight solid dark gray and light gray lines parallel to the x -axis to indicate the positions of the vertical planes depicted in Fig. 5. The images in Fig. 3 illustrate the relatively straight nature of the fireline in ambient winds of $1 m s^{-1}$, compared to those for ambient winds of $6 m s^{-1}$ and $12 m s^{-1}$. It is important to recognize that the straight nature of the fireline shown in Fig. 3a is a result of the exclusion of end effects; without excluding end effects the line would take on curvature as illustrated in Linn and Cunningham (2005). The vector field in Fig. 3a illustrates the acceleration of the horizontal winds as they move from the rear of the fire toward the front of the fire.

Fig. 3b and c illustrates the drastically different nature of the fireline structure for ambient winds of $6 m s^{-1}$ and $12 m s^{-1}$ compared to the $1 m s^{-1}$ fireline shown in Fig. 3a. The firelines in Fig. 3b and c show flow patterns and fireline shape that is indicative of coupled atmosphere–fire behavior described in other publications (Linn and Cunningham, 2005; Cunningham and Linn, 2007; Dupuy et al., in press). Of particular interest is the strongly fingered rear contour of the fireline and the undulations along the fire front that do not have the same spatial scale. The converging streams (often being initiated in the fingered tails of the fireline) and wider diverging streams of vectors (often initiated in the spaces between the fingered tails) are indicative of streamwise vortices in which heated air is pulled together and rises while cooler air is drawn down. Pockets of air are carried in a helical pattern as they move from the rear of the fireline to the front. One particular result of these flow patterns is the enhanced entrainment of fast moving air from aloft being brought down near the surface. These streamwise vortices or the helical transport patterns are precluded in a two-dimensional simulation. The difference in spatial scale of the perturbations at the rear and the front of the fireline suggest that the streamwise vortices that develop near the rear of the fireline interact with each other, and in some cases merge into larger vortices that are tilted upwards to form vertical vortices near the front of the fireline. Interestingly, the lobes of the fireline that are pushing forward with respect to the rest of the fire front are coincident with divergence in the velocity field near the ground. This suggests the presence of downdrafts, which are sometimes associated with streamwise vortices that are pulling hot gases to the surface and helping to preheat the fuels in front of the fireline. The difference in thickness of the fireline shown in Fig. 3b compared to that seen in Fig. 3c is attributed to the difference in the balance between buoyant forces and the mean wind, with the larger wind speeds in the U12y160m case stretching the fireline width more than in the U06y160m case.

3.3. Finite length fireline

Fig. 4a–c is presented to illustrate finite length fire geometries and their qualitative comparison to periodic fireline geometry. Fig. 4a–c shows fires that have ambient wind speeds of $1 m s^{-1}$, $6 m s^{-1}$, and $12 m s^{-1}$ respectively. Each of these had an initial fireline length of 100 m. These plots are the finite length analogs to those shown in Fig. 3. Fig. 4a shows a similar fireline to the one illustrated in Fig. 3a with a relatively uniform streamwise thickness. It is also interesting that both of these $1 m s^{-1}$ fire simulations produced firelines that are fairly straight. The finite length has a much more profound affect on the geometries of the $6 m s^{-1}$ and $12 m s^{-1}$ fires, illustrated in Fig. 4b and c, then the $1 m s^{-1}$ fire shown in Fig. 4a. Note that toward the center of the finite fireline the same upwind fingering is present as can be seen in the periodic firelines shown in Fig. 3b and c. However, the fingers are considerably shorter in the finite-length fires and the fingers are not as prevalent on the flanking portions of the fires. The wind vectors illustrate that in the finite cases, the winds are drawn toward the fires with vector patterns curving toward the fire perimeter on both the upstream and downstream sides. The convergence of the winds from both sides of these fires is consistent with the rising air at the site of the fireline, and the sweeping pattern around the downstream side of the fire perimeter is enabled by the wind getting around the end of the fire. In the periodic firelines, shown in Fig. 3b and c, the winds are unable to get around the ends of the fireline and thus any convergence that occurs near the base of the fire must result from air that is brought down from above the fireline.

3.4. Fireline vorticity and helical flow

An illustration of some of the effects of the streamwise vorticity patterns is presented in Fig. 5. Fig. 5 contains an image looking upstream that contains isosurfaces of potential temperature at 500 K. Superimposed on these isosurfaces are color contours of the stream-wise component of vorticity. Vorticity at the red end of the color spectrum has counterclockwise rotation relative to the view orientation provided ($-x$ vorticity). The blue end of the spectrum is indicative of clockwise rotation. Also shown is a vertical y - z plane of velocity vectors along the fire front. The top portion of Fig. 5 is half as long as the whole U06y160 fireline in the y direction. In this wide view, rising intermittent plumes of hot gas can be seen along the length of the shown fire as well as a tongue of hot gas at ground level that protrudes downstream from $x=25$ – 50 m. In addition, there is a blow up view of a section of the fireline centered around this tongue. The protruding lobe is also present in Fig. 3b near $x=280$ m, $y=40$ m. On the left side of the tongue, there is a strong clockwise rotation, while on the right side counterclockwise rotation is noted. The vector field presented in the blow up shows that air is penetrating the fireline between the hot, buoyant plumes of gas to either side of the tongue. Heated gas is rising and pulled into the counter-rotating vortex pair on both sides of the protrusion. Then the heated gases coalesce and transport forward and downward into the tongue. Since this is a continuous process, the fuel underneath the tongue heats to the point of combustion and the fire front geometry takes on the undulating lobe shapes that are apparent in Fig. 3b and c. In other words, as air penetrates the fireline, it is heated by burning fuel, and in some locations corkscrews and is transported down to the fuel in a helical path. This three-dimensional process cannot be replicated in a two-dimensional model.

3.5. Vertical fireline geometry

Figs. 6–8 each contain two images illustrating vertical x - z planes with potential temperature contours at 350 K and 400 K, and wind

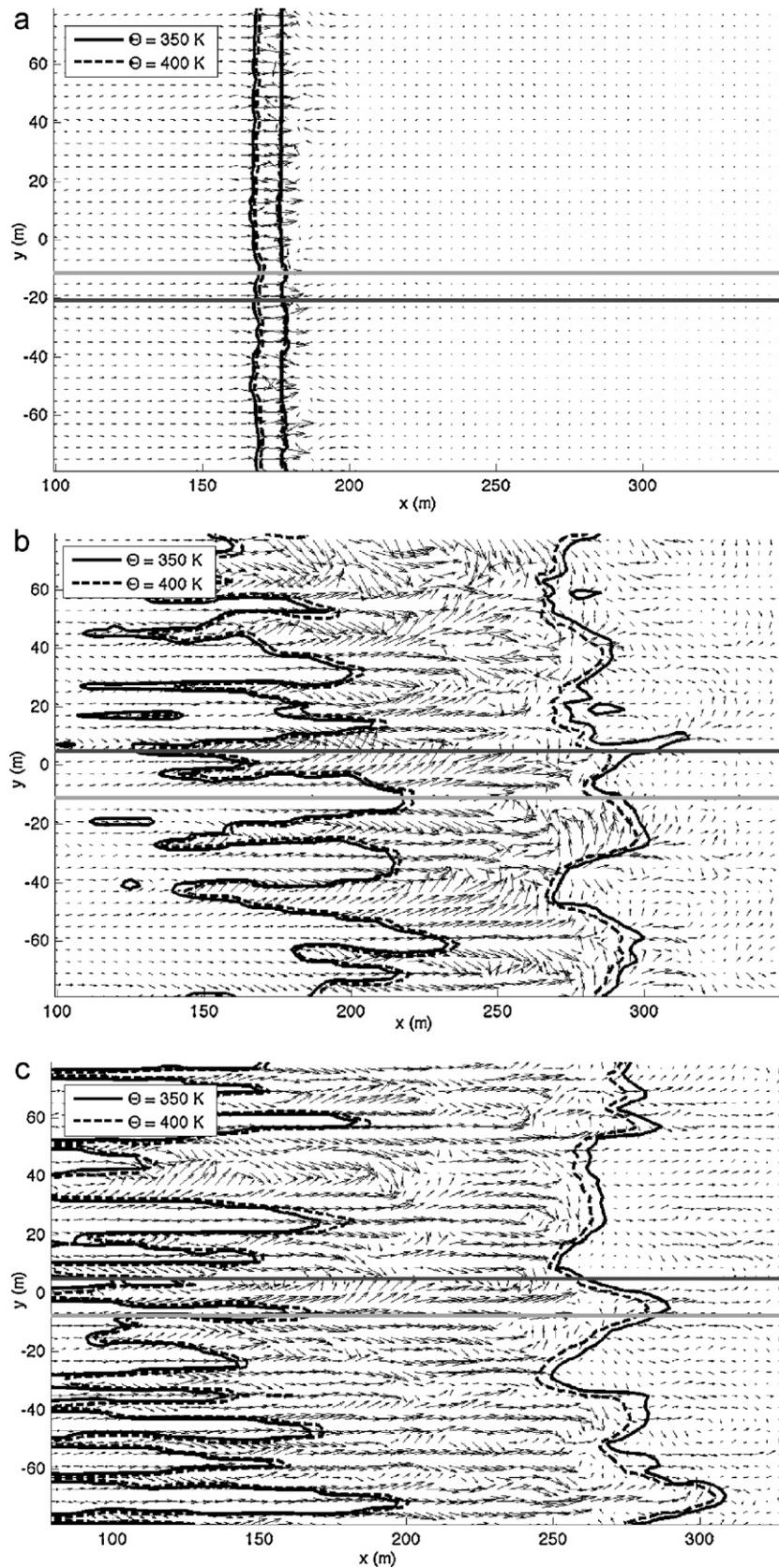


Fig. 3. These are plots of x - y slices of potential temperature in the fuel layer with velocity vectors. The solid black line represents $\theta = 350$ K, and the dashed black line is $\theta = 400$ K. The two gray, straight lines are references to Fig. 5. The dark gray line is placed in the general region of a converging wind-field at the ground and the light gray line is placed along a line of divergence in the wind-field at the ground. (a) U01y160m at $t = 800$ s, (b) U06y160m at $t = 200$ s, and (c) U12y160m at $t = 140$ s.

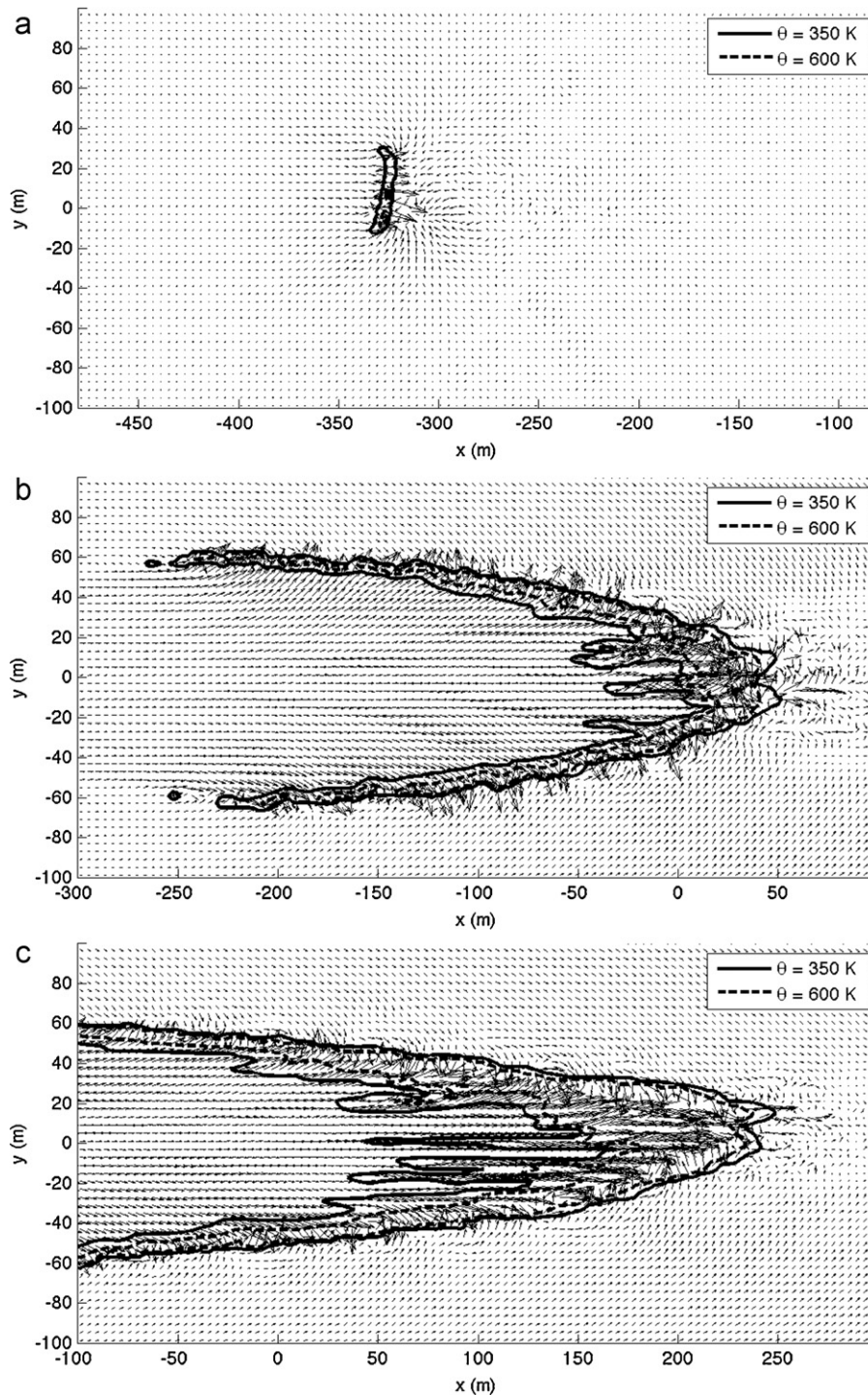


Fig. 4. These are plots of x - y slices of potential temperature in the fuel layer with velocity vectors for the finite fireline cases. The solid black line represents $\theta = 350$ K, and the dashed black line is $\theta = 600$ K. (a) U01FINITE at $t = 400$ s, (b) U06FINITE at $t = 400$ s, and (c) U12FINITE at $t = 300$ s.

vectors from the U01y160m, U06y160m and U12y160m simulations, respectively. Figs. 6a, 7a, and 8a are taken from a vertical slice positioned at a y -location within the fireline where there is convergence of the v -component of velocity near the ground (at least through part of the fireline width), corresponding to the darker gray line in Fig. 3a–c, respectively. Figs. 6b, 7b, and 8b depict vertical slices where v diverges at the ground, corresponding to the lighter gray line in Fig. 3a–c, respectively. Near the ground, the potential temperature gradient is high. This causes the contours to be close together and hard to distinguish (nearly on top of each

other in some instances of Fig. 6). This is particularly apparent for U01y160m because the hot gas region is smaller than in the other two cases.

Images from U01y160m (Fig. 6a and b) depict plumes of hot gases that have a relatively narrow base, that stand up at approximately 30° from the vertical, and that are very similar to each other. This is consistent with the relatively straight and narrow fireline seen in Fig. 3a. Inside the contours of heated gas the vectors show consistently rising air, whereas the plume above the contours is indicated by intermittent rising vectors. The intermittency

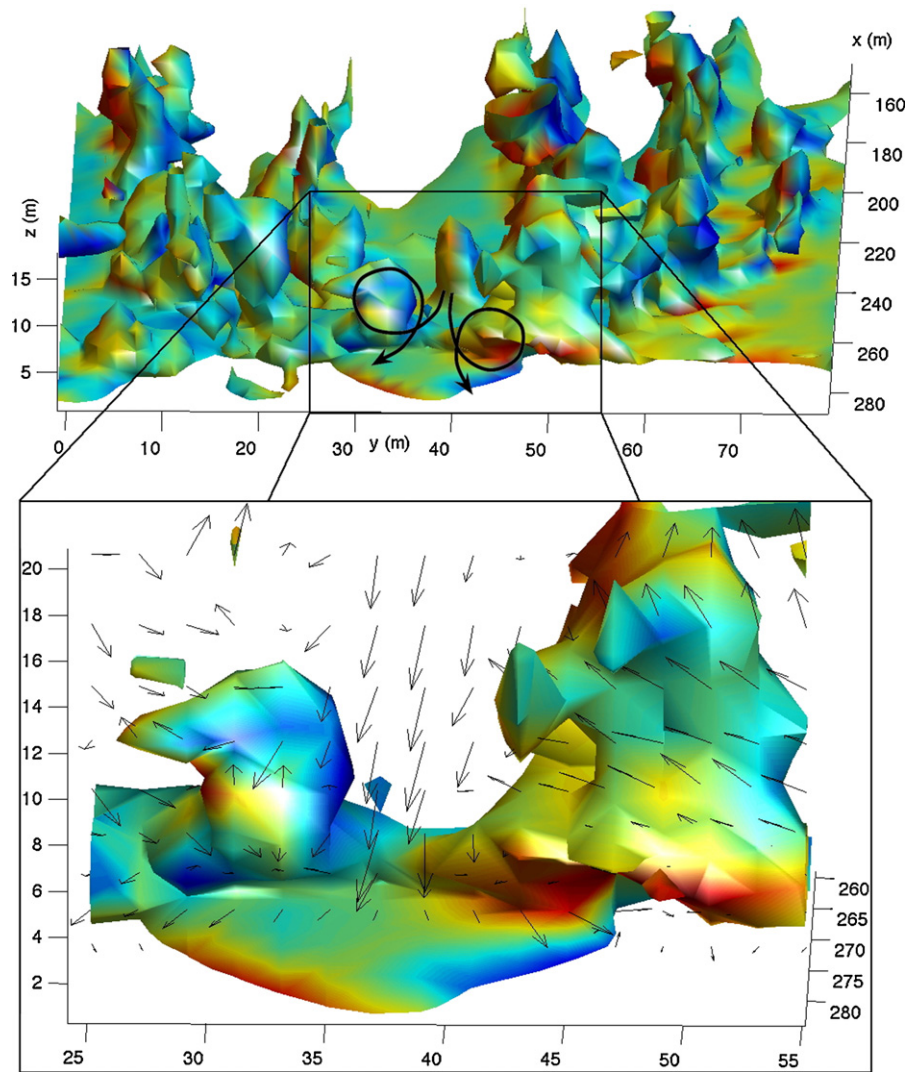


Fig. 5. Here is an isosurface of potential temperature (500 K). The color contours on the isosurface represent the streamwise component of vorticity. The red end of the spectrum depicts counterclockwise, while the blue end shows regions of clockwise rotating vortices. The vectors emphasize the velocity field.

of this rising vector pattern in the x - and z -directions is related to the three-dimensional mixing, which allows the plume to continue to rise while winds pass through the rising gas curtain. The profiles and vector patterns in Fig. 6a and b are very different in character from those seen in Figs. 7 and 8.

Fig. 7a and b illustrates the drastically different profiles of the heated plume, not only with those shown in Fig. 6, but also compared with each other. The image shown in Fig. 7a is associated with a y -location that possesses a deep zone of updrafts, whereas Fig. 7b illustrates a y -location with significant downdrafts and much shorter updraft widths than can be seen in Fig. 7a. Fig. 7a, being largely located within an updraft, is a collection zone for heated gases near the ground as they converge and rise, resulting in a wider portion of the fireline in the x -direction above 350 K than is seen in Fig. 7b, where cooler air is descending and cooling the rear of the fireline, thus leaving spaces between the fingers as seen in Fig. 3b. In Fig. 7a, the complexity of the pattern with extensive spatial variability is indicative of the three-dimensional flow pattern that includes advection of warmer and cooler gases in the cross-stream (y) direction. Fig. 7b illustrates the more predominant downdraft in this plane that extends well into the area where the ground level gases are hot.

Fig. 8a and b contains images from the U12y160m simulation, and show similarities to Fig. 7a and b in that there are wider and

narrower sections of the fireline associated with predominant updrafts and downdrafts, respectively. The higher wind speed and vertical wind shear near the surface results in a more shallow updraft region, and a more broken plume than in Fig. 7a, suggesting significant mixing and entrainment along its top edge.

3.6. Two-dimensional simulations

Fig. 9 shows three images illustrating the results from the two-dimensional calculations (U01y2D, U06y2D, and U12y2D) for comparison with the corresponding three-dimensional periodic runs depicted in Figs. 6–8, respectively. In these three two-dimensional simulations, there are no cross-flow variations in temperature or wind velocity because they are constrained to two dimensions. Comparison between these three images shows that the simulation with relatively slow ambient winds of 1 m s^{-1} has a very different appearance to those of the higher wind speed simulations (i.e., 6 m s^{-1} and 12 m s^{-1}).

Fig. 9a is similar in character to both Fig. 6a and b. This is not surprising since the similarity of Fig. 6a and b, and the straight fire front shape shown in Fig. 3a, suggested that this fire was fairly homogeneous in the y -direction (compared to fires at higher wind speeds), and thus will have similarities to the two-dimensional case. There is a notable difference between Fig. 9a and 6a and b in the height

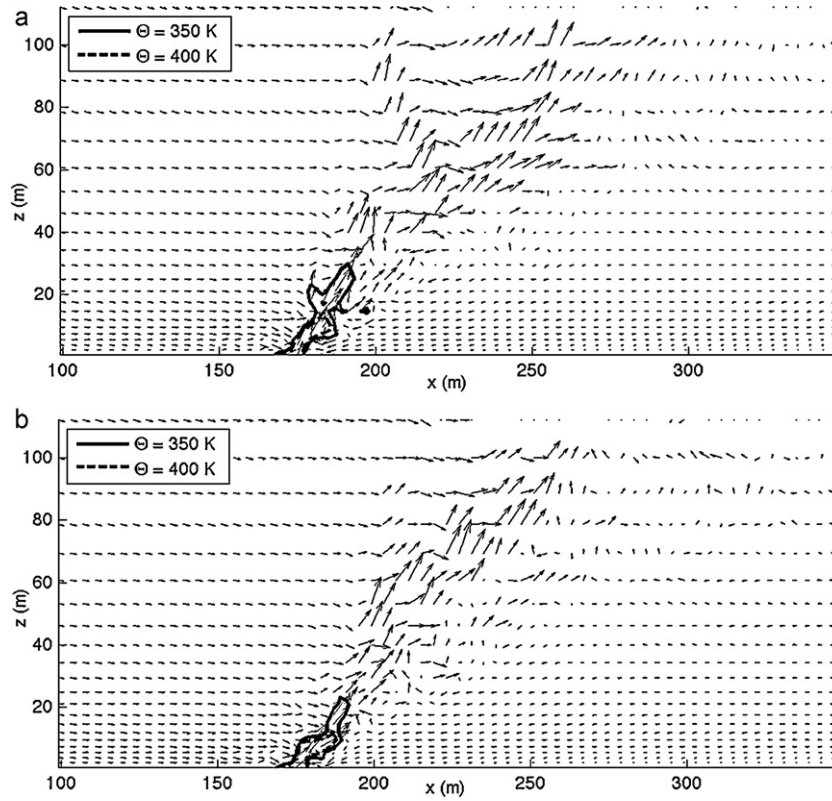


Fig. 6. Here, plots are shown of x - z slices of U01y160m at $t=800$ s with potential temperature contours and (u, w) vectors. Panel (a) is a slice aligned with the dark gray line from Fig. 3a and is a region of converging wind-field at the ground. Panel (b) is a slice aligned with the light gray line from Fig. 3a and is a region of diverging wind-field at the ground.

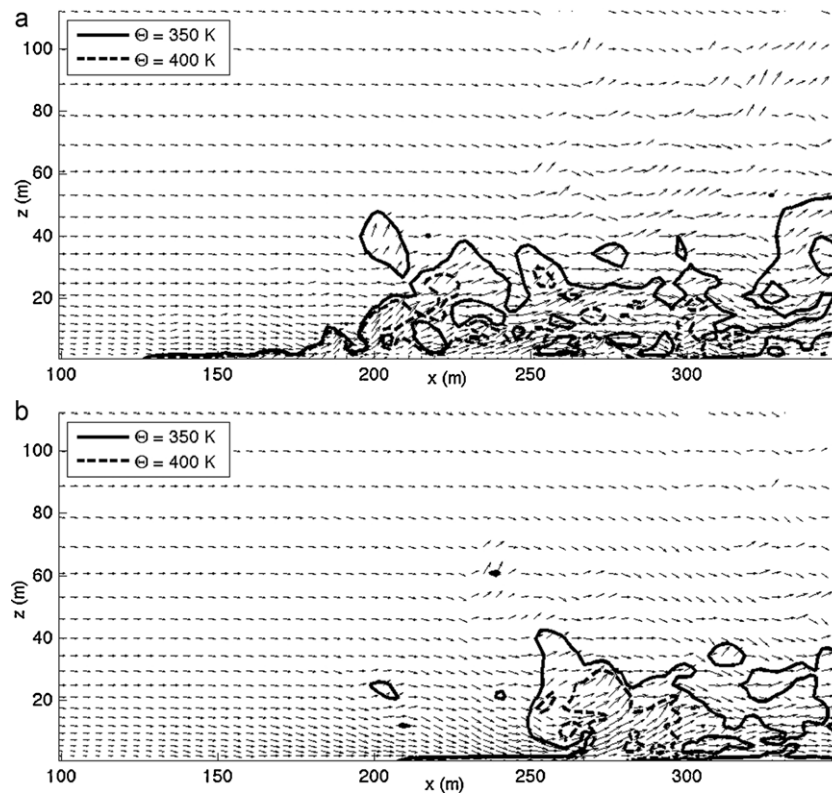


Fig. 7. These plots are representations of x - z slices of U06y160m at $t=200$ s with potential temperature contours and (u, w) vectors. Panel (a) is a slice aligned with the dark gray line from Fig. 3b and is a region of converging wind-field at the ground. Panel (b) is a slice aligned with the light gray line from Fig. 3b and is a region of diverging wind-field at the ground.

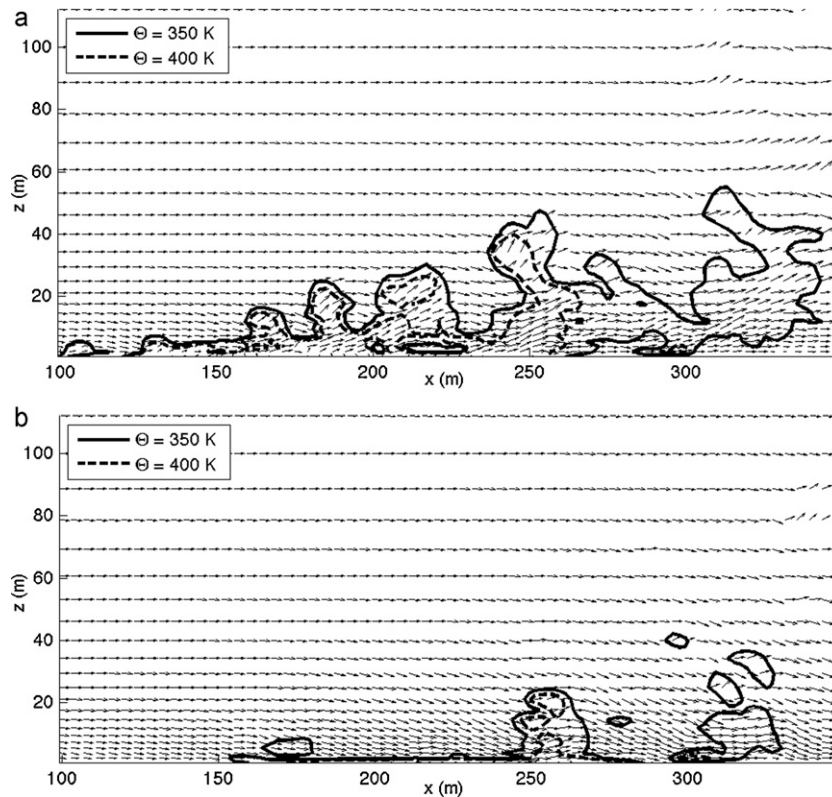


Fig. 8. Plots of x - z slices of U12y160m at $t = 140$ s with potential temperature contours and (u, w) vectors are given. Panel (a) is a slice aligned with the dark gray line from Fig. 3c and is a region of converging wind-field at the ground. Panel (b) is a slice aligned with the light gray line from Fig. 3c and is a region of diverging wind-field at the ground.

of the region with temperatures above 350 K, and this is associated with the fact that no mixing is allowed in the y -direction and thus less entrainment of cool air occurs in the two-dimensional case. There is a difference in the circulation patterns above fires at heights between 40 and 120 m above the ground as seen in a comparison of Fig. 9a with Fig. 6a and b. For the two-dimensional case, large coherent vortices can be seen in Fig. 9a above and downstream of the fire. However, in the three-dimensional case, the wind field is less structured and appears to be more disorganized in Fig. 6a and b in the same region and coherent vortices cannot easily be singled out. The difference is because, in two dimensions, vortices can only have axis in the cross-stream direction, while in the three-dimensional simulations, the flow can be in the cross-stream direction and rotation of the fluid can be about any axis. In the three-dimensional simulations, the penetration of the ambient winds through the plume creates rotation about vertical and streamwise directions as well as the cross-stream direction.

Fig. 9b depicts a very different structure than that seen in either Fig. 9a or Fig. 7. The plume in Fig. 9b has a more periodic intermittency than that seen in Fig. 7a, with very distinctive development and release of hot gas pockets at regular intervals in time. The frequency of this so-called plume “puffing” is approximately 0.2 s^{-1} . The scale of the plume structure grows due to entrainment of surrounding air as the plume is carried downstream and the released warm bubble rises in height. The entrainment becomes obvious because the bubble cools rapidly while it is expanding; the associated mushrooming motion of the plumes as they move downwind results in a downdraft on their upwind side and the side closest to the ground. This downdraft is partially responsible for heating the fuels in front of the fire as the plumes are carried downstream. The effectiveness of this rolling motion is a function of the balance between buoyancy and wind strength. The differences in

behavior between plumes in Fig. 9b and 7 is largely due to the fact that the predominant streamwise and vertical rolls in the three-dimensional simulations are not possible in the two-dimensional case, and therefore the entrainment, updrafts, and downdrafts are confined to share the single two-dimensional plane. In Fig. 9b, the downstream fireline width at the ground, evident by the 350 K contour, is approximately 100 m long in the stream-wise direction compared to a range of about 75–200 m shown in Fig. 7.

Fig. 9c is also different from the other images in Fig. 9 and its three-dimensional counterparts in Fig. 8. The large wind velocity, the associated strong vertical shear, and the entrainment that are confined to this single plane drive these differences. In Fig. 9c, it is seen that the strong wind shears the heated pockets of air and carries them downstream at regular intervals as seen in Fig. 9b; however, the increased temporal frequency, 0.33 s^{-1} , of this shearing, and the much stronger wind speed, changes the downstream heating of the fuel. The mushrooming plume behavior, including the downdraft that was very important in simulation U06y2D, is much less apparent, and as a result these heated gas pockets have very little effect on heating the fuel and spreading the fire. The fire spreads in this case by the advection of the main fire front. This is not unlike the three-dimensional case, except for the very significant impact of the cross-stream heterogeneity in the three-dimensional simulations. When cross-stream variability exists, there are locations where the winds push through the fire without fighting the buoyant rise of the plume, and in some cases they are aided by the helical patterns which carry hot faster moving gases down to the surface. Since these patterns are precluded in the two-dimensional case, the buoyant plume gas expansion and gas release in the area of the fire obstruct the advection more so than in U12y160. This explains some of the very intermittent spread patterns described by Linn (1997) and Morvan and Dupuy (1997).

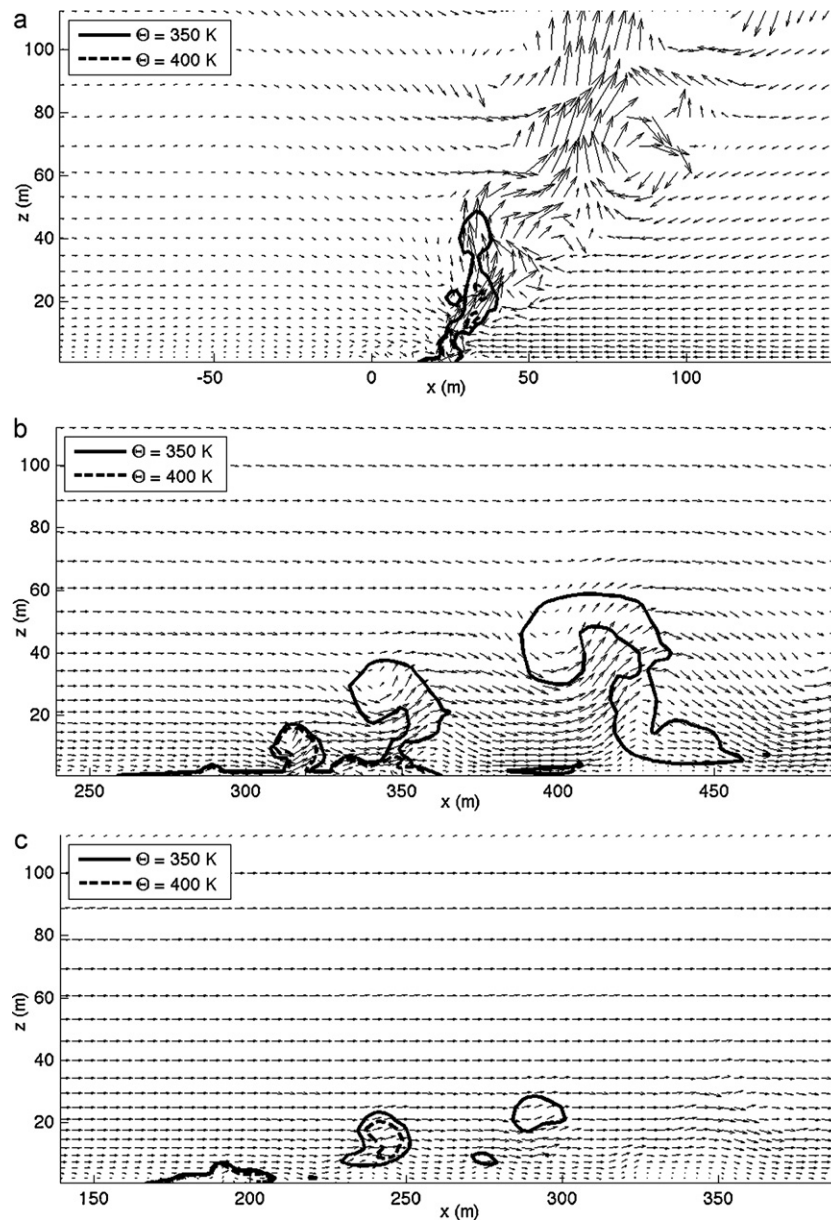


Fig. 9. These images show plots with potential temperature contours in the x - z plane with (u, w) vectors from the two-dimensional simulations. The solid black contours are lines with $\theta = 350$ K and the dashed contours are lines with $\theta = 400$ K (a) U01y2D at $t = 100$ s, (b) U06y2D at $t = 331$ s, and (c) U12y2D at $t = 268$ s.

3.7. Periodic fireline cross-stream variations

Fig. 10a–c shows slices in the y - z plane that illustrate the cross-stream variations in the periodic simulations U01y160m, U06y160m, and U12y160m, respectively. Each of these y - z slices depict color contours of the u -component of the velocity, superimposed with vectors of velocity in the plane, (v, w) . From these images, it is apparent that there is significant variability between different y -locations within the fireline, but to a lesser degree for weak ambient winds (Fig. 10a) than for stronger winds (Fig. 10b and c), consistent with the trends discussed previously. It is important to recognize that even though there is less dramatic variability along the fireline in Fig. 10a than in Fig. 10b or c, the variability still exists and allows wind to move through the plume. An example of the variability in the cross-stream direction in Fig. 10b can be seen near $y = -40$ m; the windfield shows a strong updraft in w , intense forward streamwise flow in u , and convergence near

the ground in the cross-stream velocity, v . However, 30 m away at $y = -10$ m, there is a coherent downdraft with weaker streamwise flow and divergence in v near the ground. Several of these relatively coherent updrafts and downdrafts are visible with length scales on the order of 20–30 m. Similar characteristics are also present in Fig. 10c; however, the variability seen in Fig. 10c depicts a wider range of scales with less coherence in structure at the 20–30 m scales than can be seen in Fig. 10b. This is consistent with the more intermittent patterns apparent in Fig. 8a than are present in Fig. 7a. Another feature that is visible in Fig. 10 is the collection of fireline scale vortices whose axes are aligned with the mean flow. Also in Fig. 10b, to the right of $y = 60$ m and 40 m above the ground, a strong jet in u is evident, on either side of which the contours depict a very weak u component, indicating the presence of a vortex with a vertical axis. This figure again illustrates the presence of three-dimensional aspects of the flow field.

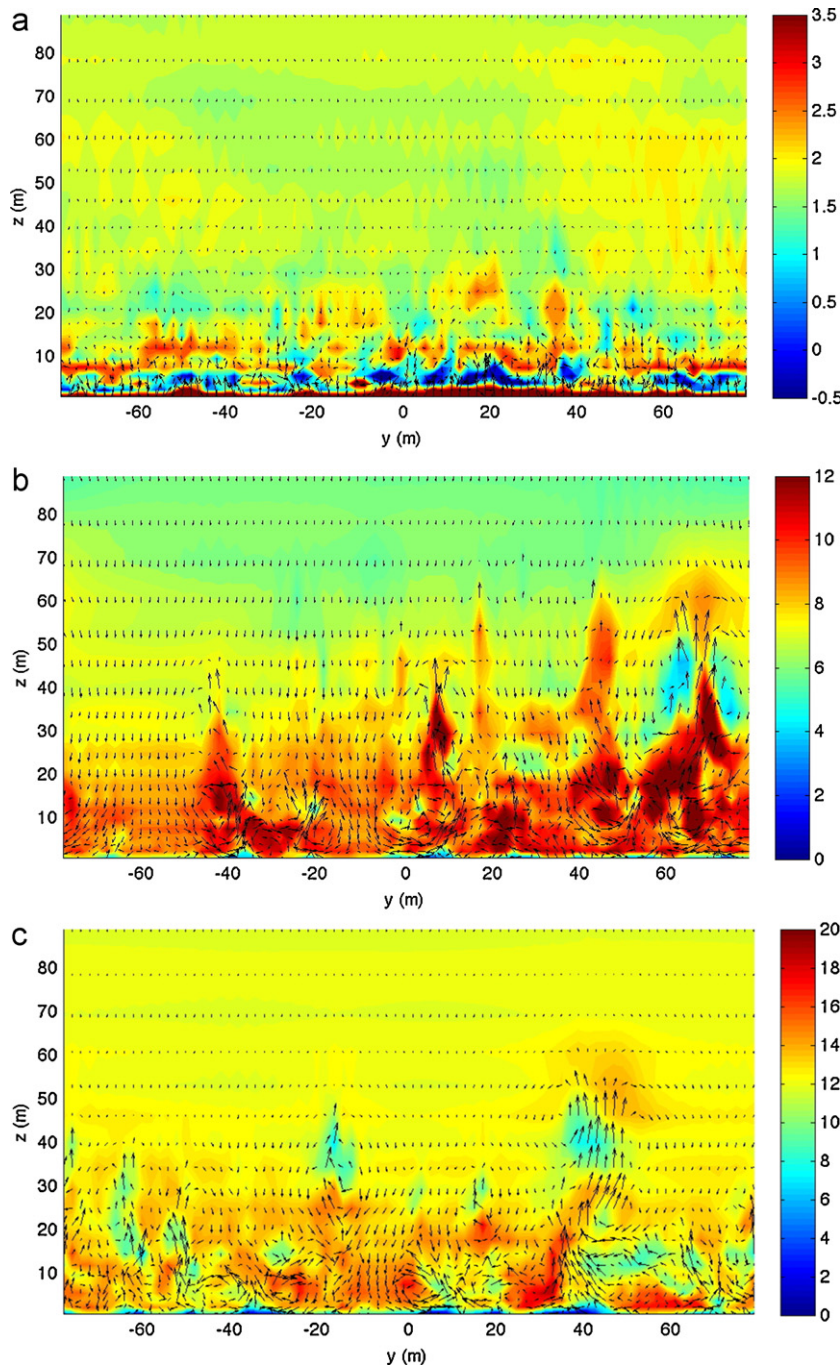


Fig. 10. Plots of y - z slices of u velocity color contours for each ambient wind speed are depicted. Vectors represent (v, w) velocities at a location downwind of the ignition. (a) $U_{01}y_{160m}$ at 173 m from ignition, (b) $U_{06}y_{160m}$ at 229 m from ignition, and (c) $U_{12}y_{160m}$ at 199 m from ignition.

3.8. Fireline rate of spread

For the purposes of discussing fire spread rates in this paper, the location of the fire front is defined as the location of the farthest downwind x -location at which the solid temperature exceeds 500 K. The movements of the fire fronts for the two-dimensional and three-dimensional periodic simulations are depicted in Fig. 11a–f for ambient winds of 1, 3, 6, 9, 12, and 15 m s^{-1} , respectively. In addition, each of these plots shows the fire front movement in five three-dimensional simulations for each ambient wind speed that have cyclic lateral boundary conditions and domain widths of 10, 20, 40, 80, and 160 m. Also for comparison purposes, a finite-length fireline, with 100 m long ignition, for each

ambient wind speed is included in these plots. The rate of spread for these simulations is estimated by following the movement of the fire front with time. The rate of spread values given in Table 2 are taken to be the slope of the least-squares linear fit to the curves in Fig. 11. This curve fit was done over the period of time that elapsed for the fire to propagate from the ignition line to a position 500 m downwind.

Fig. 11 demonstrates that allowing for the impacts of local three-dimensionality has a significant impact on the rate of fire propagation. The nature of this impact is highly dependent on wind speed, as was true for the plume structures discussed previously. Fig. 11 illustrates that for low wind speeds ($U_0 = 1 \text{ m s}^{-1}$) the absence of local three-dimensionality leads to higher rates

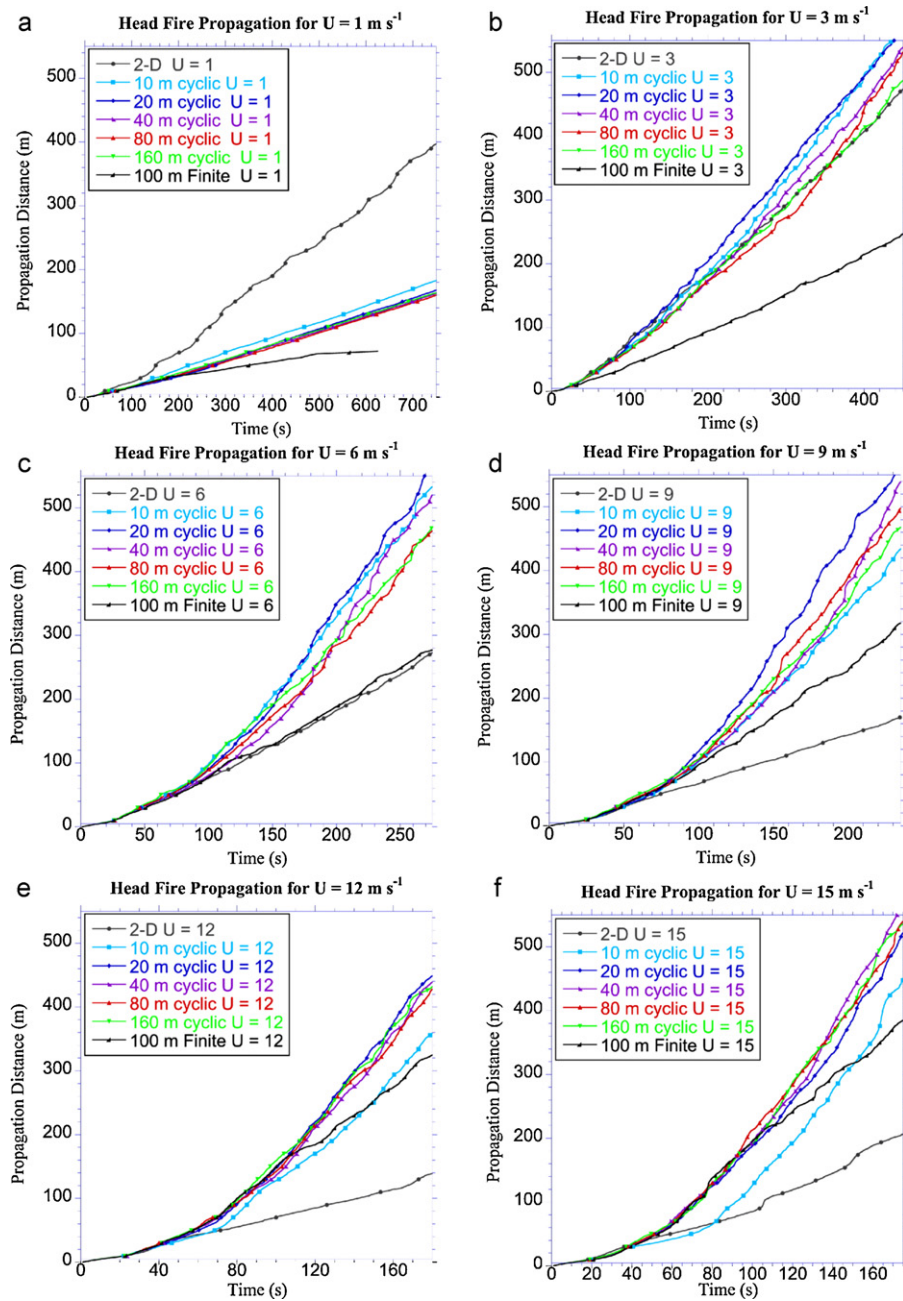


Fig. 11. Here spread distance is plotted against time for (a) $U_{01y160m}$, (b) $U_{03y160m}$, (c) $U_{06y160m}$, (d) $U_{09y160m}$, (e) $U_{12y160m}$, and (f) $U_{15y160m}$.

of spread than are observed in the three-dimensional periodic simulations (Fig. 11a), while at higher wind speeds this absence leads to slower rates of spread in the two-dimensional cases than are seen in the three-dimensional periodic simulations (Fig. 11b–f). Based on the results and discussion presented above, it appears that this is related to the wind pushing on the plume at low wind speeds without being able to finger through the lower portions of the plume in the two-dimensional case. This effect is similar to that of pressure on an obstacle in cross-flow, since the winds are unable to penetrate through the lower region of the plume, and the pressure pushes the fire forward at a faster rate than it could if it were able to penetrate through the plume (allowed by cross-flow variations seen in Fig. 10). At high wind speeds in the two-dimensional simulations, the warm bubbles are sheared off from the ground level fire and begin to rise. Once these heated bubbles begin to rise they are not effective at heating the unburned

fuel, while in the three-dimensional calculations with higher wind speeds, the penetration of the gases through the fireline incites significant downdrafts and helical transport of fast-moving hot gas to the ground. Thus the locally three-dimensional fires spread faster than they do in the corresponding two-dimensional case.

Fig. 11 also illustrates that for domain widths greater than 10 m, the width of the domain has a diminishing impact on the propagation of the fire front or on the net rate of spread. This result is also summarized in Table 2 in the form of the rates of spread for the various widths of the three-dimensional periodic domains. The first implication of this result is that for the periodic simulations, the scale of the important local three-dimensional atmosphere–fire coupling becomes independent of the domain width as the domain becomes large enough. Conversely, when the domain is too narrow and the cross-stream scale restrictions limit the nature of the three-dimensional flow patterns, the spread rates would be affected. With

a wind speed of 15 m s^{-1} , the 10 m wide simulation spreads initially as though its three-dimensional flow is constrained, similar to the corresponding two-dimensional case, while after about 80 s it begins to spread at a similar rate to the other periodic fires. The second implication of this result is that it is not as important to extend the domain width beyond this critical value in order to estimate spread rates of an infinitely long fireline. It is important to point out that these statements regarding the local three-dimensional effects do not reflect on the importance of larger fireline-scale (non local) three-dimensional effects such as line length or curvature.

Although this paper is focused on the influence of local three-dimensionality, the propagation curves for 100 m long firelines are included for purposes of comparison. These finite-length firelines are similar in character to those described by Linn and Cunningham (2005), except for the difference between inlet wind profiles and therefore surface wind speeds. The details of the implications of the finite-length versus infinite-length firelines will be described in subsequent papers; however, the important fundamental difference should be noted. Finite-length firelines allow winds to access the ambient air upstream of the fireline without penetrating through the fire, thus altering aspects of the indraft on both sides of the fire and the shape of the fire, which in turn affects the convective and radiative heat transfer. The result of these differences is largely to slow the fire spread. Indeed, in Fig. 11 for each wind speed, the finite-length fireline is slower than the infinite-length fireline by the end of the simulations.

Fig. 12 shows the spread rates of all of the simulations as a function of ambient wind speed. Two critical points are highlighted by this figure. First, it illustrates that the two-dimensional fireline simulations predict higher spread rates than the finite-length firelines for ambient winds of 1, 3, and 6 m s^{-1} , but significantly lower spread rates for ambient winds of 9, 12, and 15 m s^{-1} , as mentioned above. The rate of spread reaches a local maximum in this plot for ambient wind speeds in the range of 6 m s^{-1} , then the spread rate dips to a local minimum between wind speeds of 9 and 12 m s^{-1} before it increases again for higher wind speeds. These results mimic those obtained by Morvan and Dupuy (1997). Second, it demonstrates that although the magnitude of the infinitely long periodic fireline spread rates are greater than those of the finite-length firelines for the same ambient winds, both finite-length firelines and periodic firelines show the same increasing trends with wind speed. These

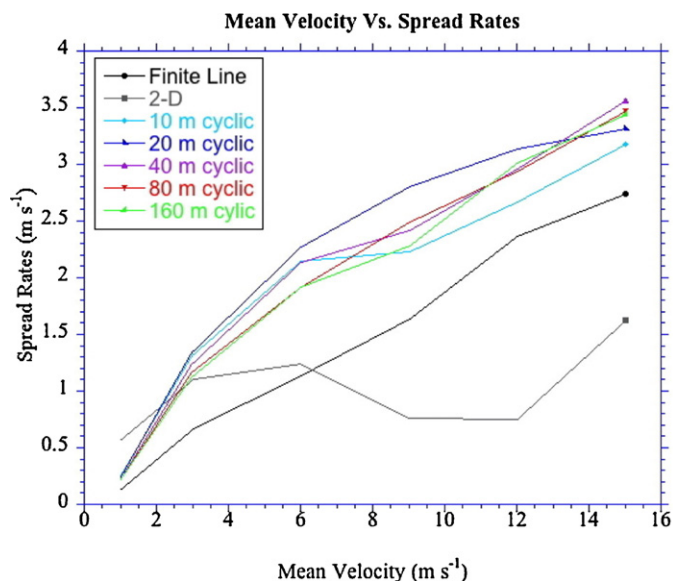


Fig. 12. Here is a plot of free-stream (ambient) velocity against spread rate for all scenarios.

trends are similar to those illustrated in Linn and Cunningham (2005) for 16 m and 100 m firelines. End effects include both the effects on radiation view factors that occur at the ends of the fireline and, potentially more importantly, effects of fireline curvature and the flow of air around the fireline that is then entrained in front of the fire (i.e., fireline scale vertical vorticity). It is understandable that the impacts of end effects and curvature would become less important as the length of the firelines increases.

The magnitude of the variation between the spread rates for a given ambient wind speed across the various periodic simulations is relatively small for 1 m s^{-1} , suggesting that the scale for the local three-dimensional flow and plume structures is generally less than 10 m in the cross-stream direction. For larger wind speeds this variation increases, suggesting that the scales of the turbulent flow structures are broader and are affected by the limitations of even the 80 m wide domain. Variations in rate of spread are similar for all wind speeds larger than 1 m s^{-1} . If the 10 m periodic case were omitted, relative variations are smaller at the largest wind speeds (12 and 15 m s^{-1}) than at 3, 6, and 9 m s^{-1} wind speeds. In fact, the largest variations in spread rates occurs in the $6\text{--}9 \text{ m s}^{-1}$ window, suggesting that there is a transition in flow characteristics present in this range.

4. Summary and conclusions

4.1. Simulations

In this paper, a coupled atmosphere–fire model (HIGRAD/FIRETEC) was employed to investigate the influence of local three-dimensionality of the coupled atmosphere–fire dynamics associated with fire behavior in grasslands. In order to perform this investigation, a series of three-dimensional simulations were performed using periodic boundary conditions in the cross-stream direction (i.e., parallel to the fireline). Fires were ignited over the entire width of the domain, which was taken to be one of 10, 20, 40, 80, or 160 m. In addition, two-dimensional and three-dimensional finite-length (100 m) fireline simulations were performed for comparison. Six different ambient wind speeds were chosen for each of the two-dimensional, three-dimensional periodic, and three-dimensional finite-length fireline simulations. The structures of the velocity and temperature fields were studied in a subset of the simulations spanning the wind speeds for both the three-dimensional periodic and two-dimensional cases. Propagation and spread rate trends were also examined in order to improve understanding of the impacts of local three-dimensionality and the implications of two-dimensional assumptions.

The use of cyclic or periodic conditions on the lateral boundaries of the simulations serves to remove the effects of global fire shape or end effects, and allowed this investigation to focus on local three-dimensionality. This was an effective approach; however, a comparison with finite-length firelines reminds us of the significance of the additional fireline-scale three-dimensional factors that should be considered when trying to understand spread rates as a function of environmental conditions.

4.2. Three-dimensional effects

It was shown that the nature of the atmosphere–fire coupling changes with wind speed, as does the variability along the length of the fireline. At ambient wind speeds of 1 m s^{-1} , there is variation along the length of the fireline, but the fireline is fairly straight and the spread rate is independent of the width of the domain (for domains greater than 10 m wide). This result suggests that the spanwise variations have length scales that are typically less than 10 m. At ambient wind speeds above 1 m s^{-1} , the rear of the

fireline is fingered and the front of the fireline exhibits significant lobes, while the velocity field shows strong evidence of stream-wise vortices that interact with each other and in some cases take on vertical components near the fire front. The average spread rates for the different domain widths vary by approximately 20%, indicating that there is some effect of the constraints that the cyclic boundary conditions impose and that there is a variety of sizes of atmosphere–fire structures that affect the spread rates. At ambient wind speeds of 12 m s^{-1} , the structure of the wind and temperature fields also show evidence of streamwise vortices, although the structures illustrated by vector fields and temperature contours are more complex and less coherent, and have a wider variation of their scales. The variation of the spread rate based on the width of the domain is also about 20%, again suggesting a wide variety of influential scales.

When the fires were simulated under a two-dimensional assumption, thus precluding cross-stream variation, the influence of the restriction to two dimensions was also dependent on wind speed. At ambient wind speeds of 1 m s^{-1} , the general structure of the plume was not qualitatively different from those seen in the three-dimensional periodic simulation, but the spread rate was more than twice as fast. For higher wind speeds, the effect of the two-dimensional assumption changes significantly due to the preclusion of the vorticity structures and the ability of the wind to mix through the heated plume and entrain hot gases down into the fuels ahead of the fire. As a result, there is a much slower spread rate in the two-dimensional simulations compared to the periodic three-dimensional simulations for ambient winds of 6 m s^{-1} and higher.

4.3. Rates of spread

For the three-dimensional simulations, the increase of spread rate with wind speed is similar to that reported in previous publications, including Linn and Cunningham (2005), but the magnitude of the spread rates for the periodic simulations were in general larger than seen in the finite-length fireline simulations. This result should be the basis for subsequent explorations concerning the influence of end effects and fireline shape, which are additional forms of three-dimensionality that were not the focus of this paper.

4.4. Concluding remarks

The results of this study indicate that caution should be exercised when attempting to invoke a two-dimensional assumption for wildland fire spread, especially when attempting to use such an assumption in the context of a process-based model such as that of Linn (1997). Care should be taken to account for the combined impacts of the variations in the flow field and plume structure in the third dimension. It is possible that this could be incorporated in a manner similar to how turbulence kinetic energy and effective mixing are modeled without actually resolving them; however, this is not a trivial task and has not been attempted to date.

Acknowledgments

Portions of this work were supported by the USDA Forest Service Rocky Mountain Research Station under the direction of Carleton Edminster and Carolyn Sieg, David Weise and the Joseph W. Jones Ecological Research Center at Ichaaway under the direction of Kevin Hiers and Lindsay Boring. The computational resources for this study were provided by Los Alamos National Laboratory Institutional Computing.

References

- Alexander, M.E., Steffner, C.N., Mason, J.A., Stocks, B.J., Hartley, G.R., Maffey, M.E., Wotton, B.M., Taylor, S.W., Lavoie, N., Dalrymple, G.N., 2004. Characterizing the Jack Pine-Black Spruce Fuel Complex of the International Crown Fire Modelling Experiment (ICFME). Information Report NOR-X-393. Northern Forestry Centre, Canadian Forest Service.
- Baines, P.G., 1990. Physical mechanisms for the propagation of surface fires. *Mathematical and Computational Modelling* 13, 83–94.
- Beer, T., 1991. The interaction of wind and fire. *Boundary-Layer Meteorology* 54, 287–308.
- Beer, T., 1993. The speed of a fire front and its dependence on wind speed. *International Journal of Wildland Fire* 3, 193–202.
- Bossert, J.E., Linn, R.R., Reisner, J.M., Winterkamp, J.L., Dennison, P., Roberts, D., 2000. Coupled atmosphere–fire behavior model sensitivity to spatial fuels characterization. In: *Third Symposium on Fire and Forest Meteorology*. American Meteorological Society.
- Bradley, M., 2002. This model can take the heat. <http://www.lnl.gov/str/November02/Bradley.html>.
- Brown, J., Arno, S., 1991. The paradox of wildland fire. *Western Wildlands* Spring, 40–46.
- Burgan, R.E., 1988. Revisions to the 1978 National Fire-Danger Rating System. Research Paper SE-273. USDA Forest Service, Asheville, North Carolina.
- Carrier, G.F., Fendell, F.E., Wolff, M.F., 1991. Wind-aided firespread across arrays of discrete fuel elements. I. Theory. *Combustion Science and Technology* 75, 31–51.
- Cassagne, N., Pimont, F., Dupuy, J.L., Linn, R.R., Mârell, A., Oliveri, C., Rigolot, E., 2011. Using a fire propagation model to assess the efficiency of prescribed burning in reducing the fire hazard. *Ecological Modelling* 222, 1502–1514.
- Catchpole, W.R., Catchpole, E.A., Butler, B.W., Rothermel, R.C., Morris, G.A., Latham, D.J., 1998. Rate of spread of free-burning fires in woody fuels in a wind tunnel. *Combustion Science and Technology* 131, 1–37.
- Cheney, N.P., Gould, J.S., 1995. Fire growth in grassland fuels. *International Journal of Wildland Fire* 5, 237–244.
- Cheney, N.P., Gould, J.S., Catchpole, W.R., 1993. The influence of fuel, weather and fire shape variables on fire-spread in grasslands. *International Journal of Wildland Fire* 3, 31–44.
- Cheney, N.P., Gould, J.S., Catchpole, W.R., 1998. Prediction of fire spread in grasslands. *International Journal of Wildland Fire* 8, 1–13.
- Colman, J.J., Linn, R.R., 2007. Separating combustion from pyrolysis in HIGRAD/FIRETEC. *International Journal of Wildland Fire* 16, 493–502.
- Cunningham, P., Linn, R.R., 2007. Numerical simulations of grass fires using a coupled atmosphere–fire model: dynamics of fire spread. *Journal of Geophysical Research* 112, D05108, doi:10.1029/2006JD007638.
- Cunningham, P., Goodrick, S.L., Hussaini, M.Y., Linn, R.R., 2005. Coherent vortical structures in numerical simulations of buoyant plumes from wildland fires. *International Journal of Wildland Fire* 14, 61–75.
- Dupuy, J.L., Larini, M., 1999. Fire spread through a porous forest fuel bed: a radiative and convective model including fire-induced flow effects. *International Journal of Wildland Fire* 9, 155–172.
- Dupuy, J.L., Linn, R.R., Kononov, V., Pimont, F., Vega, J., Jiménez, E., 2011. Exploring three-dimensional coupled fire/atmosphere interactions downwind of wind-driven surface fires and their influence on backfiring using the HIGRAD-FIRETEC model. *International Journal of Wildland Fire* 20, 734–750.
- Finney, M.A., 1998. FARSITE: Fire Area Simulator – Model Development and Evaluation. Research Paper RMRS-RP-4. USDA Forest Service, Ogden, Utah.
- Grishin, A.M., 1997. *Mathematical Modeling of Forest Fires and New Methods of Fighting Them*. Publishing House of the Tomsk State University, Tomsk, Russia.
- Koo, E., Pagni, P., Woycheese, J., Stephens, S., Weise, D., Huff, J., 1997. A simple physical model for forest fire spread rate. In: *Fire Safety Science: Proceedings of the Eighth International Symposium*, pp. 851–862.
- Larini, M., Giroud, F., Porterie, B., Loraud, J.C., 1998. A multiphase formulation for fire propagation in heterogeneous combustible media. *International Journal of Heat and Mass Transfer* 41, 881–897.
- Linn, R.R., Cunningham, P., 2005. Numerical simulations of grass fires using a coupled atmosphere–fire model: basic fire behavior and dependence on wind speed. *Journal of Geophysical Research* 110, D13107, doi:10.1029/2004JD005597.
- Linn, R.R., Harlow, F.H., 1998. Mixing-limited transport model used for description of wildfires. In: *Computational Technologies for Fluid/Thermal/Structural/Chemical Systems With Industrial Applications*. ASME, New York, pp. 161–168.
- Linn, R.R., Reisner, J.M., Colman, J.J., Winterkamp, J., 2002. Studying wildfire behavior using FIRETEC. *International Journal of Wildland Fire* 11, 233–246.
- Linn, R.R., Winterkamp, J., Colman, J.J., Edminster, C., Bailey, J.D., 2005a. Modeling interactions between fire and atmosphere in discrete element fuel beds. *International Journal of Wildland Fire* 14, 37–48.
- Linn, R.R., Canfield, J.M., Winterkamp, J.L., Cunningham, P., Coleman, J.J., Edminster, C., Goodrick, S.L., 2005b. Numerical simulations of fires similar to the International Crown Fire Modeling Experiment. In: *Proceedings of the American Meteorological Society: Sixth Symposium on Fire and Forest Meteorology and 19th Interior West Fire Council Meeting*.
- Linn, R.R., Winterkamp, J., Edminster, C., Colman, J.J., Smith, W.S., 2007. Coupled influences of topography and wind on wildland fire behavior. *International Journal of Wildland Fire* 16, 183–195.

- Linn, R.R., Winterkamp, J., Weise, D., Edminster, C., 2010. A numerical study of slope and fuel structure effects on coupled wildfire behavior. *International Journal of Wildland Fire* 19, 179–201.
- Linn, R.R., 1997. A transport model for prediction of wildfire behavior. Sci. Rep. LA-13334-T. Los Alamos National Laboratory, Los Alamos, New Mexico.
- Margerit, J., Séro-Guillaume, O., 2002. Modelling forest fires, part ii: reduction to two-dimensional models and simulation of propagation. *International Journal of Heat and Mass Transfer* 45, 1723–1737.
- Mell, W., Jenkins, M.A., Gould, J., Cheney, P., 2007. A physics-based approach to modeling grassland fires. *International Journal of Wildland Fire* 16, 1–22.
- Morvan, D., Dupuy, J.L., 1997. Modeling the propagation of a wildfire through a Mediterranean shrub using a multiphase formulation. *Combustion and Flame* 138, 199–210.
- Morvan, D., Dupuy, J.L., 2001. Modeling of fire spread through a forest fuel bed using a multiphase formulation. *Combustion and Flame* 127, 1981–1994.
- Parsons, R.A., 2007. *Spatial Variability in Forest Fuels: Simulation Modeling and Effects on Fire Behavior*. University of Montana.
- Pimont, F., Linn, R.R., Dupuy, J.L., Morvan, D., 2006. Effects of vegetation description parameters on forest fire behaviour with FIRETEC. *Forest Ecology and Management* 234S, S120.
- Pimont, F., Dupuy, J.L., Linn, R.R., Dupont, S., 2009. Validation of FIRETEC wind-flows over a canopy and a fuel-break. *International Journal of Wildland Fire* 18, 775–790.
- Pimont, F., Dupuy, J.L., Linn, R.R., Dupont, S., 2011. Impact of tree canopy structure on wind-flows and fire propagation simulated with FIRETEC. *Annals of Forest Sciences* 68, 523–530.
- Reisner, J.M., Wynne, S., Margolin, L., Linn, R.R., 2000. Coupled atmospheric–fire modeling employing the method of averages. *Monthly Weather Review* 128, 3683–3691.
- Rothermel, R.C., 1972. A mathematical model for predicting fire spread in wildland fuels. Research Paper INT-115. USDA Forest Service, Ogden, Utah.
- Weise, D.R., 1993. *Modelling wind and slope-induced wildland fire behavior*. Ph.D. Thesis. University of California, Berkeley.
- Wolff, M.F., Carrier, G.F., Fendell, F.E., 1991. Wind-aided firespread across arrays of discrete fuel elements. II. Experiment. *Combustion Science and Technology* 77, 261–289.
- Zhou, X., Weise, D.R., Mahalingam, S., 2005. Experimental measurements and numerical modeling of marginal burning in live chaparral fuel beds. *Proceedings of the Combustion Institute* 30, 2287–2294.